

# Accurate and efficient computation of mean ionization states with an average-atom Kubo–Greenwood approach

Timothy J. Callow,<sup>1, 2, \*</sup> Eli Kraisler,<sup>3, †</sup> and Attila Cangj<sup>1, 2, ‡</sup>

<sup>1</sup>*Center for Advanced Systems Understanding (CASUS), D-02826 Görlitz, Germany*

<sup>2</sup>*Helmholtz-Zentrum Dresden-Rossendorf, D-01328 Dresden, Germany*

<sup>3</sup>*Fritz Haber Center for Molecular Dynamics and Institute of Chemistry,*

*The Hebrew University of Jerusalem, 9091401 Jerusalem, Israel*

(Dated: March 14, 2022)

The mean ionization state (MIS) is a critical property in dense plasma and warm dense matter research. Unfortunately however, the best way to compute the MIS remains an open question. Average-atom (AA) models are widely-used due to their computational efficiency, but we show that the canonical approach for calculating the MIS in AA models is typically insufficient. However, we demonstrate that an approach which uses the Kubo–Greenwood conductivity formula in an AA model yields excellent agreement with both higher fidelity simulations and experimental data.

Warm dense matter (WDM) is a phase of matter characterized by temperatures on the order of  $1 - 100$  eV and densities of  $10^{-2} - 10^4$  g cm $^{-3}$  [1, 2]. Under these conditions, conventional divisions between solid-state and plasma physics are bridged and a variety of interesting phenomena emerge, including for example non-equilibrium effects [3], phase transitions [4, 5], and partially ionized matter. WDM is observed in various astrophysical domains, such as exoplanets [6] and brown and white dwarfs [7, 8]; furthermore, during inertial confinement fusion (ICF), materials are exposed to WDM conditions [9, 10].

The mean ionization state (MIS), or equivalently the free electron density, is of particular importance in WDM. It is directly related to physical properties such as electrical conductivity, opacity, collision rates and acoustic velocities [11, 12]. Furthermore, the MIS is an input parameter for various simulations including hydrodynamics [13] and Monte–Carlo simulations [14], finite-temperature pseudo-potentials for density-functional theory calculations [15, 16], and in computing adiabats used in ICF modelling [10]. Additionally, accurate predictions of the MIS are crucial for validating and fitting models to experimental data [17, 18].

In the WDM regime, there is rarely a clear distinction between ‘bound’ and ‘free’ electrons, meaning the MIS is hard to define. The ramifications of this ambiguity extend beyond direct computation of the MIS: they are relevant to recent debates regarding the ionization potential depression (IPD) effect [19–22], and further raise questions regarding the application of the Chihara decomposition [23–25]. These difficulties are further compounded by the variety of methods used in the modelling of WDM, running all the way from analytical models such as Stewart–Pyatt [26] and Ecker–Kroll [27] to *ab initio* density-functional theory (DFT) [28–32] and path-integral Monte–Carlo [33, 34] simulations.

Average-atom (AA) models are a popular and successful tool in modelling the WDM regime, since they incor-

porate in a natural way quantum effects (typically using DFT) at a manageable computational cost [35–37]. There is a wide range of AA models [38], but they share in common the concept of an atom immersed in a plasma. Typically, the MIS is defined as the number of electronic states with energy above a certain threshold,

$$\bar{Z} = \int_{v(R_{\text{WS}})}^{\infty} g(\epsilon) f_{\text{FD}}(\epsilon), \quad (1)$$

where  $g(\epsilon)$  denotes the density-of-states and  $f_{\text{FD}}(\epsilon)$  the Fermi–Dirac (FD) distribution, and  $v(R_{\text{WS}})$  the value of the mean-field potential at the boundary at the Wigner–Seitz radius  $R_{\text{WS}}$ .

As seen in a previous work [38], the definition (1) is somewhat limited, showing large discrepancies for different choices of boundary condition and sharp discontinuities when  $\bar{Z}$  is plotted as a function of temperature or density. Furthermore, bound and free states in AA models are typically treated differently, and hence the definition of  $\bar{Z}$  is both an output of and input to the model, which means any errors may self-multiply. We note however that modern AA models do not always follow this assumption [39, 40].

DFT molecular dynamics (DFT-MD) simulations can also be used to compute the MIS using definition (1) (with the threshold energy typically assumed to start at the conduction band lower edge). In DFT-MD simulations, all (non-core) orbitals are treated on the same footing. Even so, the definition (1) is limited because it assumes states can be categorized as completely bound or completely free based on their energy alone, and DFT-MD results have shown divergence from experimental measurements [17].

Consequently, novel ways of computing the MIS have recently gained traction. For example, Bethkenhagen *et al.* proposed using the Kubo–Greenwood (KG) conductivity formula to measure the MIS [11]. The comparison of their results with an AA model showed significant differences in the MIS. However, pressures computed with

the AA and DFT-MD models were in excellent agreement [41], which suggests that a more pertinent definition of  $\bar{Z}$  in the AA model might give better agreement.

In this Letter, we adapt the KG method of Ref. 11 to an AA model. This approach shows excellent agreement both with DFT-MD simulations [11] and experimental data [42–44], is highly computationally efficient, and is free from empirical input. Additionally, we explore two other approaches for computing the MIS with an AA model. Firstly, we use the canonical definition (1), which (as expected) gives inconsistent results, particularly for high densities. Secondly, we introduce a novel approach which uses the electron localization function (ELF) to determine the MIS. The ELF has been used extensively in quantum chemistry and materials science [45, 46], but to the best of our knowledge has not been applied to study ionization in WDM. We shall see that this method yields more consistent and accurate results, compared to the canonical approach, but the best agreement with the benchmarks comes from the KG-AA method.

*Theory* — The AA model we use follows from the model derived in Ref. 38. We direct the reader to this previous paper and the Supplementary Material for a detailed description of our AA model, and here restrict our discussion to only the key features and differences from the previous model. In our AA model, we solve the Kohn–Sham DFT (KS-DFT) equations for a single atom consisting of a nucleus with charge  $Z$  and a fixed number of electrons  $N_e$  (with  $N_e = Z$  for all the systems we consider). Explicit interactions between this atom and its neighbours are ignored, and instead these interactions are implicitly accounted for via boundary conditions. Unlike in Ref. 38, in which the ‘bound’ and ‘unbound’ orbitals were treated differently, in the current work we solve the same KS equations for *all* orbitals, regardless of their energy. The orbitals  $X_{nl}(r)$  must obey one of the following boundary conditions: (i)  $X_{nl}(R_{\text{WS}}) = 0$ , (ii)  $dX_{nl}(r)/dr|_{R_{\text{WS}}} = 0$ , which we shall henceforth refer to as respectively the “Dirichlet” (i) and “Neumann” (ii) boundary conditions.

Furthermore, to extend our comparisons beyond the model described above, we have implemented the AA model proposed by Massacrier *et al.* In this model, the KS equations are solved for *both* the Dirichlet and Neumann boundary conditions, yielding energies  $\epsilon_{nl}^{\pm}$  which define the upper (Dirichlet) and lower (Neumann) limits of a band-structure, with the DOS approximated by the Hubbard function [47]. In the Supplementary Material, we demonstrate good qualitative agreement between the DOS from this AA model and a DFT-MD benchmark [11].

The Kubo–Greenwood (KG) conductivity formula for

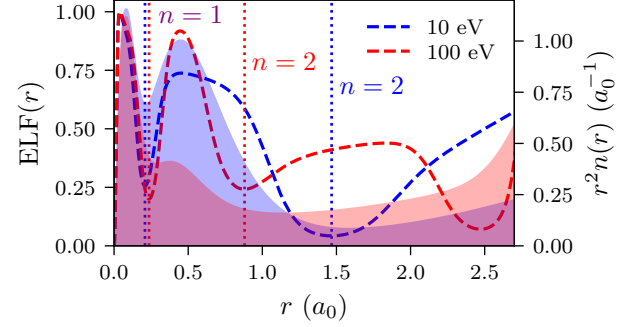


FIG. 1. The ELF (dashed) and radial density distribution (shaded) for Aluminium at its ambient density  $\rho_m = 2.7 \text{ g cm}^{-3}$ , at two different temperatures  $\tau = 10$  and  $100 \text{ eV}$ .

a finite system is given by [48, 49]

$$\sigma_{S_1, S_2}(\omega) = \frac{2\pi}{3V\omega} \sum_{i \in S_1} \sum_{j \in S_2} (f_i - f_j) |\langle \phi_i | \nabla | \phi_j \rangle|^2 \times \delta(\epsilon_j - \epsilon_i - \omega), \quad (2)$$

where  $S_1$  and  $S_2$  denote a chosen subset of orbitals (for example the orbitals in the conduction band),  $V$  is the volume of the system under consideration,  $\phi_i$  are the KS orbitals and  $\epsilon_i$  and  $f_i$  are their energies and FD occupations. For the total conductivity,  $S_1$  and  $S_2$  represent the complete set of orbitals.

As described in Ref. [11], Eq. (2) can be used as a proxy for the mean ionization state in combination with the Thomas–Reiche–Kuhn (TRK) sum rule [50–52]

$$\bar{Z} = \frac{2V}{\pi} \int_0^\infty d\omega \sigma_{c,c}(\omega), \quad (3)$$

where  $\sigma_{c,c}$  means both orbital subsets are given by the conducting orbitals. If the total conductivity  $\sigma_{t,t}(\omega)$  is used in place of the conducting part only, then the total electron number  $N_e (= Z)$  should be recovered. This provides a useful check of the implementation and convergence. The KG formula for spherically symmetric orbitals is derived in Ref. [49] and is also given in the Supplementary Material.

In KS-DFT, the usual expression for the (total density) electron localization function (ELF) is given by [45, 53]

$$\text{ELF}(\mathbf{r}) = \frac{1}{1 + [D(\mathbf{r})/D_0(\mathbf{r})]^2}, \quad (4)$$

where  $D(\mathbf{r})$  and  $D_0(\mathbf{r})$  are the electron pair density curvature (EPDC) functions for the system and for the uniform electron gas (UEG) respectively. We have found that an approximate expression for the kinetic energy density in  $D(\mathbf{r})$ , based on a second-order gradient expansion [54], yields more clearly identifiable minima in the ELF than the normal orbital-dependent expression. This

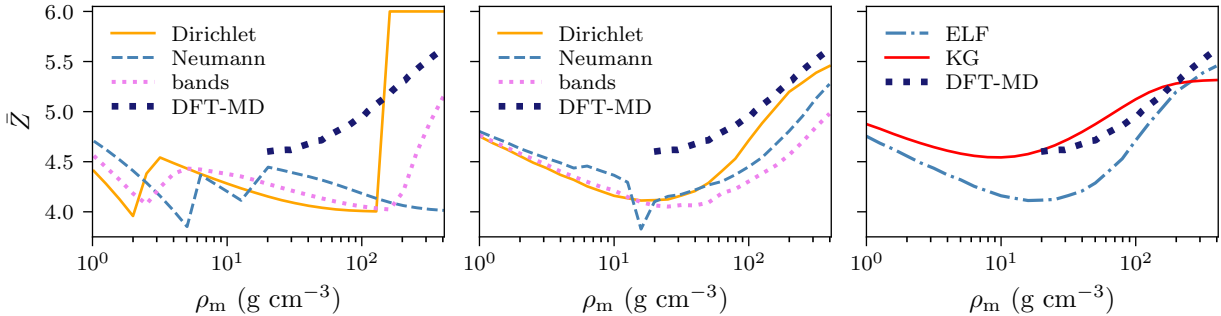


FIG. 2. Comparison of different models for the mean ionization state (MIS) of Carbon with temperature 100 eV as a function of density. DFT-MD data is taken from Ref. [11] and uses the Kubo-Greenwood method. Left: comparison of boundary conditions with the MIS computed with the energy threshold method. Centre: comparison of boundary conditions with the MIS computed via the ELF. Right: comparison of different methods for computing the MIS with the Dirichlet boundary condition.

density-based expression for  $\tau(\mathbf{r})$  leads to the following expression for the EPDC  $D(\mathbf{r})$

$$D(\mathbf{r}) = D_0(\mathbf{r}) - \frac{1}{9} \frac{|\nabla n(\mathbf{r})|^2}{n(\mathbf{r})} + \frac{1}{6} \nabla^2 n(\mathbf{r}). \quad (5)$$

The EPDC for the UEG is given by the usual expression  $D_0(\mathbf{r}) = (3/10)(3\pi^2)^{2/3} n^{5/3}(\mathbf{r})$ . The ELF is therefore bounded in the range  $0 \leq \text{ELF}(r) \leq 1$ , and is thus a quantitative measure of electron localization.

The ELF has a long history in quantum chemistry [45, 46, 53] as a tool for understanding atomic structure and chemical bonding. Integrating the electron density between the minima of the ELF indicates the number of electrons in a particular atomic shell. We propose to use the ELF as a measure of the MIS by computing the number of electrons per shell, and assuming that any electron density beyond a particular shell (pre-determined using physical intuition and examination of the DOS) is free. In Fig. 1, we compare the ELF and radial density distribution  $r^2 n(r)$  for Aluminium at its ambient density  $\rho_m = 2.7 \text{ g cm}^{-3}$ , for two different temperatures  $\tau = 10$  and 100 eV. It can be seen from this figure how the different shells are defined, and that at the higher temperature the density migrates out of the  $n = 1, 2$  shells.

*Results* — All calculations have been performed using the open-source average atom code atoMEC [55]. The numerical implementation follows to a large extent what we had described in a previous paper [38] and is described in detail in the Supplementary Material. We acknowledge several scientific libraries and methods critical to the development of atoMEC [56–61].

In the following, we shall compare the three methods described for computing the MIS — the canonical or “threshold” approach (1), the KG method (2) and the technique based on the ELF — against a higher fidelity DFT-MD benchmark and experimental data. For the threshold and ELF results, we compare the Dirichlet and

Neumann boundary conditions and the band-structure model. For the KG results, we use the Dirichlet boundary condition only. This is because the sum rule check for the total conductivity is observed very accurately (within 1%) across all conditions for the Dirichlet boundary condition, but not for the others; we are investigating possible reasons for this. We use throughout the (spin-unpolarized) local density approximation (LDA) for the xc-functional [62].

First, we compare our results with the DFT-MD simulations for Carbon Ref. 11 in Fig. 2. In the left-hand sub-plot, we plot the canonical threshold method for each of the boundary conditions. We see that this method has severe limitations, especially at the highest densities, when the three boundary conditions yield diverging results. Furthermore, in the density-range in which the DFT-MD simulations were performed, none of the AA results are remotely close to the reference result.

In the central sub-plot of Fig. 2, we plot the MIS obtained via the ELF method against the DFT-MD benchmark. In order to obtain these results, we took the electron density in the  $n = 1$  sub-shell to be bound, and everything outside it to be free. We see that this approach yields a more realistic picture for the MIS, as the results from the three boundary conditions are at least consistent and capture the correct qualitative behaviour; however, they all systematically under-estimate the MIS relative to the DFT-MD result.

Finally, in the right-hand sub-plot of Fig. 2, we compare the ELF and KG results using the Dirichlet boundary condition with the DFT-MD simulation. Here we observe very strong agreement between our AA model and the DFT-MD benchmark for the KG result. Only at the very highest densities do we see some divergence between the results. In Ref. [11], it was postulated that the AA result deviates from the DFT-MD result because the AA model does not account for the many-body interactions. Based on Fig. 2, there is encouraging evidence

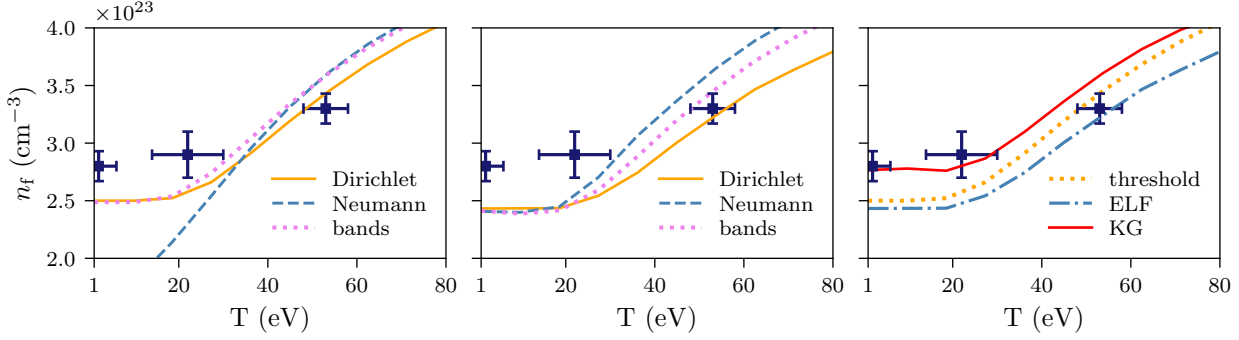


FIG. 3. Comparison of different models and experimental data [42] for the free electron density as a function of temperature for solid-density Beryllium ( $\rho = 1.85 \text{ g cm}^{-3}$ ). Left: comparison of boundary conditions with the MIS computed with the energy threshold method. Centre: comparison of boundary conditions with the MIS computed via the ELF. Right: comparison of different methods for computing the MIS with the Dirichlet boundary condition.

that if the same theory is used to calculate the MIS for the AA and DFT-MD simulations, then the agreement is much better.

Next, we perform a similar set of comparisons for Beryllium in Fig. 3, this time with fixed density equal to its ambient density ( $\rho_m = 1.85 \text{ g cm}^{-3}$ ) from temperatures between  $1 - 80 \text{ eV}$ . This time, the benchmark results (shown as the 3 scattered points with error bars) are taken from an experiment, in which the free electron density  $n_f$  (which is directly related to the MIS) was determined using X-ray scattering [42]. Like in the prior Carbon example, we have assumed under these conditions that the electron density in the  $n = 1$  sub-shell is bound, and everything outside it is free.

Again, the threshold results are shown in the left-hand sub-plot and the ELF results in the centre. This time, we see better agreement between the threshold results for the different boundary conditions, although the Neumann result is significantly different from the others at low temperatures. The ELF results are somewhat similar, but resolve this inconsistency at low temperatures. Whilst both techniques seem to capture roughly the right shape of the curve and agree quite well with the highest-temperature experimental measurement, they do not agree with the other two experimental results.

In the right-hand sub-plot of Fig. 3, we compare all three approaches for computing the MIS (threshold, ELF and KG) with just the Dirichlet boundary condition against the experimental data. Strikingly, the KG results are in very close agreement with the lower temperature experimental results, although slightly over-predict the free electron density at the highest temperature. The KG result for the lowest temperature ( $\tau \approx 2 \text{ eV}$ ) is particularly interesting, because it is the only method which correctly predicts the experimentally measured value of  $\approx 2.8 \times 10^{23} \text{ cm}^{-3}$ : this is higher than the value which we might naively expect if we take ambient density Beryllium to have two free electrons per atom, which corre-

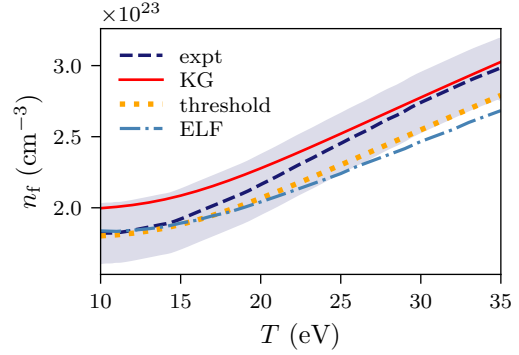


FIG. 4. Comparison of the free electron density between our AA model and experimental results [43], for Aluminium at its ambient density ( $2.7 \text{ g cm}^{-3}$ ), as a function of temperature. The shaded region represents the experimental error bars.

sponds to  $n_f = 2.5 \times 10^{23} \text{ cm}^{-3}$ .

The final comparisons we make are with a pair of experiments, both involving Aluminium at its ambient density ( $2.7 \text{ g cm}^{-3}$ ). We now focus on results using just the Dirichlet boundary condition. In the first experiment [43], the free electron density and electron temperature were measured. We compare our AA results for the three different methods with the experimental data in Fig. 4. In fact, under these conditions, all three methods largely lie within the experimental error bars, suggesting the AA model is accurate under these conditions regardless of how we measure the MIS.

In the second experiment [44], the free electron density was not itself measured, but rather the  $K$ -shell ionization energy for different charge states. We use this data indirectly to compare our methods for calculating the MIS: for a range of temperatures ( $1 - 100 \text{ eV}$ ) we compute the MIS and use this as a proxy for the charge state. We then take the  $K$ -edge ionization energy as the energy required to excite the  $1s$  orbital to

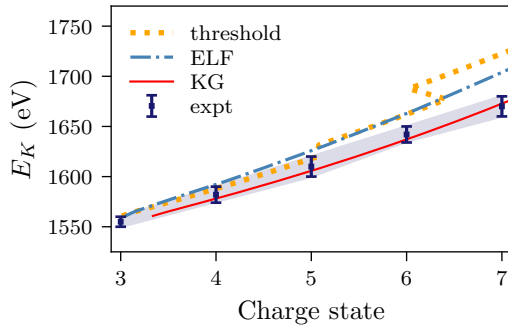


FIG. 5. Comparison of our AA model and experimental data [44] for the  $K$ -shell excitation energy as a function of the charge state for ambient-density Aluminium ( $\rho = 2.7 \text{ g cm}^{-3}$ ).

the continuum (assuming  $\epsilon_c = v_s(R_{\text{WS}})$ ). We also follow Ref. [39] and shift the orbital energy by a constant equal to the difference between  $\epsilon_{1s} - \epsilon_c$  and the experimentally measured  $K$ -shell ionization energy zero temperature, so  $E_K = \epsilon_{1s} - \epsilon_c + \Delta E_K^0$ . This comparison is shown in Fig. 5: we see here that the KG results lie consistently within the experimental range, whereas the ELF and threshold results do not (and in the case of the threshold result, there is a discontinuity). This follows from the tendency of the threshold and ELF methods to underestimate the MIS.

*Conclusions* — In this Letter, we have explored different ways of computing the mean ionization state (MIS) — a critical property in warm dense matter and dense plasmas — using a KS-DFT average-atom model. Our most important finding is that using a Kubo–Greenwood approach for computing the MIS, as first proposed in Ref. [11] using DFT-MD simulations, yields excellent agreement with both experimental data and the DFT-MD benchmark. This is of particular interest because our AA code can typically run on a laptop in the time-scale of minutes — far less computationally demanding than DFT-MD simulations.

## ACKNOWLEDGEMENTS

We thank Gérard Massacrier for useful discussions regarding the band-structure AA model. We are also grateful to the organizers of the “Average atom models for warm dense matter workshop” at UC Berkeley in June 2021, which motivated the idea for this paper. This work was partly funded by the Center for Advanced Systems Understanding (CASUS) which is financed by Germany’s Federal Ministry of Education and Research (BMBF) and by the Saxon Ministry for Science, Culture and Tourism (SMWK) with tax funds on the basis of the budget approved by the Saxon State Parliament.

\* t.callow@hzdr.de

† eli.kraisler@mail.huji.ac.il

‡ a.cangi@hzdr.de

- [1] *Basic Research Needs for High Energy Density Laboratory Physics* (U.S. DOE, 2009).
- [2] M. Bonitz, T. Dornheim, Z. A. Moldabekov, S. Zhang, P. Hamann, H. Kähler, A. Filinov, K. Ramakrishna, and J. Vorberger, Ab initio simulation of warm dense matter, *Physics of Plasmas* **27**, 042710 (2020), <https://doi.org/10.1063/1.5143225>.
- [3] Y. Ping, D. Hanson, I. Koslow, T. Ogitsu, D. Prendergast, E. Schwegler, G. Collins, and A. Ng, Broadband dielectric function of nonequilibrium warm dense gold, *Phys. Rev. Lett.* **96**, 255003 (2006).
- [4] M. D. Knudson, M. P. Desjarlais, A. Becker, R. W. Lemke, K. R. Cochrane, M. E. Savage, D. E. Bliss, T. R. Mattsson, and R. Redmer, Direct observation of an abrupt insulator-to-metal transition in dense liquid deuterium, *Science* **348**, 1455 (2015).
- [5] M. Kandyla, T. Shih, and E. Mazur, Femtosecond dynamics of the laser-induced solid-to-liquid phase transition in aluminum, *Phys. Rev. B* **75**, 214107 (2007).
- [6] U. Kramm, N. Nettelmann, J. J. Fortney, R. Neuhauser, and R. Redmer, Constraining the interior of extrasolar giant planets with the tidal Love number  $k_2$  using the example of HAT-P-13b”, *A & A* **538**, 8 (2012).
- [7] W. B. Hubbard, T. Guillot, J. I. Lunine, A. Burrows, D. Saumon, M. S. Marley, and R. S. Freedman, Liquid metallic hydrogen and the structure of brown dwarfs and giant planets, *Phys. Plasmas* **4**, 2011 (1997).
- [8] G. Chabrier, P. Brassard, G. Fontaine, and D. Saumon, Cooling sequences and color-magnitude diagrams for cool white dwarfs with hydrogen atmospheres, *Astrophys. J.* **543**, 216 (2000).
- [9] J. D. Lindl, P. Amendt, R. L. Berger, S. G. Glendinning, S. H. Glenzer, S. W. Haan, R. L. Kauffman, O. L. Landen, and L. J. Suter, The physics basis for ignition using indirect-drive targets on the National Ignition Facility, *Phys. Plasmas* **11**, 339 (2004).
- [10] A. L. Kritcher, T. Döppner, C. Fortmann, T. Ma, O. L. Landen, R. Wallace, and S. H. Glenzer, In-flight measurements of capsule shell adiabats in laser-driven implosions, *Phys. Rev. Lett.* **107**, 015002 (2011).
- [11] M. Bethkenhagen, B. B. L. Witte, M. Schörner, G. Röpke, T. Döppner, D. Kraus, S. H. Glenzer, P. A. Sterne, and R. Redmer, Carbon ionization at gigabar pressures: An ab initio perspective on astrophysical high-density plasmas, *Phys. Rev. Research* **2**, 023260 (2020).
- [12] S. H. Glenzer, W. Rozmus, B. J. MacGowan, K. G. Estabrook, J. D. De Groot, G. B. Zimmerman, H. A. Baldis, J. A. Harte, R. W. Lee, E. A. Williams, and B. G. Wilson, Thomson scattering from high-  $Z$  laser-produced plasmas, *Phys. Rev. Lett.* **82**, 97 (1999).
- [13] L. G. Stanton and M. S. Murillo, Ionic transport in high-energy-density matter, *Phys. Rev. E* **93**, 043203 (2016).
- [14] J. Vorberger and D. Gericke, Effective ion–ion potentials in warm dense matter, *High Energy Density Physics* **9**, 178 (2013).
- [15] F. Perrot and M. W. C. Dharma-wardana, Equation of state and transport properties of an interacting multiespecies plasma: Application to a multiply ionized al

- plasma, Phys. Rev. E **52**, 5352 (1995).
- [16] M. W. C. Dharma-wardana, Static and dynamic conductivity of warm dense matter within a density-functional approach: Application to aluminum and gold, Phys. Rev. E **73**, 036401 (2006).
- [17] E. García Saiz, G. Gregori, D. O. Gericke, J. Vorberger, B. Barbrel, R. J. Clarke, R. R. Freeman, S. H. Glenzer, F. Y. Khattak, M. Koenig, O. L. Landen, D. Neely, P. Neumayer, M. M. Notley, A. Pelka, D. Price, M. Roth, M. Schollmeier, C. Spindloe, R. L. Weber, L. van Woerkom, K. Wünsch, and D. Riley, Probing warm dense lithium by inelastic x-ray scattering, Nature Physics **4**, 940 (2008).
- [18] D. Kraus, B. Bachmann, B. Barbrel, R. W. Falcone, L. B. Fletcher, S. Frydrych, E. J. Gamboa, M. Gauthier, D. O. Gericke, S. H. Glenzer, S. Göde, E. Granados, N. J. Hartley, J. Helfrich, H. J. Lee, B. Nagler, A. Ravasio, W. Schumaker, J. Vorberger, and T. Döppner, Characterizing the ionization potential depression in dense carbon plasmas with high-precision spectrally resolved x-ray scattering, Plasma Physics and Controlled Fusion **61**, 014015 (2018).
- [19] S. X. Hu, Continuum lowering and fermi-surface rising in strongly coupled and degenerate plasmas, Phys. Rev. Lett. **119**, 065001 (2017).
- [20] C. A. Iglesias, A plea for a reexamination of ionization potential depression measurements, High Energy Density Physics **12**, 5 (2014).
- [21] C. A. Iglesias and P. A. Sterne, Comment on “continuum lowering and fermi-surface rising in strongly coupled and degenerate plasmas”, Phys. Rev. Lett. **120**, 119501 (2018).
- [22] S. X. Hu, Hu replies:, Phys. Rev. Lett. **120**, 119502 (2018).
- [23] J. Chihara, Difference in x-ray scattering between metallic and non-metallic liquids due to conduction electrons, Journal of Physics F: Metal Physics **17**, 295 (1987).
- [24] J. Chihara, Interaction of photons with plasmas and liquid metals - photoabsorption and scattering, Journal of Physics: Condensed Matter **12**, 231 (1999).
- [25] A. D. Baczevski, L. Shulenburger, M. P. Desjarlais, S. B. Hansen, and R. J. Magyar, X-ray thomson scattering in warm dense matter without the chihara decomposition, Phys. Rev. Lett. **116**, 115004 (2016).
- [26] J. C. Stewart and K. D. Pyatt Jr, Lowering of ionization potentials in plasmas, The Astrophysical Journal **144**, 1203 (1966).
- [27] G. Ecker and W. Kröll, Lowering of the ionization energy for a plasma in thermodynamic equilibrium, Phys. Fluids **6**, 62 (1963).
- [28] P. Hohenberg and W. Kohn, Inhomogeneous electron gas, Phys. Rev. **136**, B864 (1964).
- [29] W. Kohn and L. J. Sham, Self-consistent equations including exchange and correlation effects, Phys. Rev. **140**, A1133 (1965).
- [30] N. D. Mermin, Thermal properties of the inhomogenous electron gas, Phys. Rev. **137**, A: 1441 (1965).
- [31] M. P. Desjarlais, Density-functional calculations of the liquid deuterium Hugoniot, reshock, and reverberation timing, Phys. Rev. B **68**, 064204 (2003).
- [32] B. Holst, R. Redmer, and M. P. Desjarlais, Thermo-physical properties of warm dense hydrogen using quantum molecular dynamics simulations, Phys. Rev. B **77**, 184201 (2008).
- [33] K. P. Driver and B. Militzer, All-electron path integral Monte Carlo simulations of warm dense matter: Application to water and carbon plasmas, Phys. Rev. Lett. **108**, 115502 (2012).
- [34] T. Dornheim, S. Groth, and M. Bonitz, The uniform electron gas at warm dense matter conditions, Phys. Rep. **744**, 1 (2018).
- [35] R. P. Feynman, N. Metropolis, and E. Teller, Equations of state of elements based on the generalized Fermi-Thomas theory, Phys. Rev. **75**, 1561 (1949).
- [36] B. F. Rozsnyai, Relativistic Hartree-Fock-Slater calculations for arbitrary temperature and matter density, Phys. Rev. A **5**, 1137 (1972).
- [37] D. A. Liberman, Self-consistent field model for condensed matter, Phys. Rev. B **20**, 4981 (1979).
- [38] T. J. Callow, E. Kraisler, S. B. Hansen, and A. Cangi, First-principles derivation and properties of density-functional average-atom models (2021), accepted for publication in Phys. Rev. Research, arXiv:2103.09928 [cond-mat.mtrl-sci].
- [39] S.-K. Son, R. Thiele, Z. Jurek, B. Ziaja, and R. Santra, Quantum-mechanical calculation of ionization-potential lowering in dense plasmas, Phys. Rev. X **4**, 031004 (2014).
- [40] G. Massacrier, M. Böhme, J. Vorberger, F. Soubiran, and B. Militzer, Reconciling ionization energies and band gaps of warm dense matter derived with ab initio simulations and average atom models, Phys. Rev. Research **3**, 023026 (2021).
- [41] G. Faussurier, C. Blancard, and M. Bethkenhagen, Carbon ionization from a quantum average-atom model up to gigabar pressures, Phys. Rev. E **104**, 025209 (2021).
- [42] S. H. Glenzer, G. Gregori, R. W. Lee, F. J. Rogers, S. W. Pollaine, and O. L. Landen, Demonstration of spectrally resolved x-ray scattering in dense plasmas, Phys. Rev. Lett. **90**, 175002 (2003).
- [43] S. M. Vinko, O. Cricosta, T. R. Preston, D. S. Rackstraw, C. R. D. Brown, T. Burian, J. Chalupský, B. I. Cho, H.-K. Chung, K. Engelhorn, R. W. Falcone, R. Fiokovinini, V. Hájková, P. A. Heimann, L. Juha, H. J. Lee, R. W. Lee, M. Messerschmidt, B. Nagler, W. Schlotter, J. J. Turner, L. Vysin, U. Zastrau, and J. S. Wark, Investigation of femtosecond collisional ionization rates in a solid-density aluminium plasma, Nature Communications **6**, 6397 (2015).
- [44] O. Cricosta, S. M. Vinko, H.-K. Chung, B.-I. Cho, C. R. D. Brown, T. Burian, J. Chalupský, K. Engelhorn, R. W. Falcone, C. Graves, V. Hájková, A. Higginbotham, L. Juha, J. Krzywinski, H. J. Lee, M. Messerschmidt, C. D. Murphy, Y. Ping, D. S. Rackstraw, A. Scherz, W. Schlotter, S. Toleikis, J. J. Turner, L. Vysin, T. Wang, B. Wu, U. Zastrau, D. Zhu, R. W. Lee, P. Heimann, B. Nagler, and J. S. Wark, Direct measurements of the ionization potential depression in a dense plasma, Phys. Rev. Lett. **109**, 065002 (2012).
- [45] M. Kohout and A. Savin, Atomic shell structure and electron numbers, International Journal of Quantum Chemistry **60**, 875 (1996), <https://onlinelibrary.wiley.com/doi/10.1002/>.
- [46] P. Fuentealba, E. Chamorro, and J. C. Santos, Chapter 5 understanding and using the electron localization function, in *Theoretical Aspects of Chemical Reactivity*, Theoretical and Computational Chemistry, Vol. 19, edited by A. Toro-Labbé (Elsevier, 2007) pp. 57–85.

- [47] J. Hubbard and B. H. Flowers, Electron correlations in narrow energy bands iii. an improved solution, *Proceedings of the Royal Society of London. Series A. Mathematical and Physical Sciences* **281**, 401 (1964).
- [48] W. Johnson, C. Guet, and G. Bertsch, Optical properties of plasmas based on an average-atom model, *Journal of Quantitative Spectroscopy and Radiative Transfer* **99**, 327 (2006), *radiative Properties of Hot Dense Matter*.
- [49] L. Calderín, V. Karasiev, and S. Trickey, Kubo–greenwood electrical conductivity formulation and implementation for projector augmented wave datasets, *Computer Physics Communications* **221**, 118 (2017).
- [50] W. Thomas, Über die zahl der dispersionselektronen, die einem stationären zustande zugeordnet sind. (vorläufige mitteilung), *Naturwissenschaften* **13**, 627 (1925).
- [51] F. Reiche and W. Thomas, Über die zahl der dispersionselektronen, die einem stationären zustand zugeordnet sind, *Zeitschrift für Physik* **34**, 510 (1925).
- [52] W. Kuhn, Über die gesamtstärke der von einem zustande ausgehenden absorptionslinien, *Zeitschrift für Physik* **33**, 408 (1925).
- [53] A. D. Becke and K. E. Edgecombe, A simple measure of electron localization in atomic and molecular systems, *The Journal of Chemical Physics* **92**, 5397 (1990), <https://doi.org/10.1063/1.458517>.
- [54] V. Tsirelson and A. Stash, Determination of the electron localization function from electron density, *Chemical Physics Letters* **351**, 142 (2002).
- [55] T. Callow, D. Kotik, E. Tsvetoslavova Stankulova, E. Kraisler, and A. Cangi, atoMEC (2021), <https://doi.org/10.5281/zenodo.5205718>.
- [56] C. R. Harris, K. J. Millman, S. J. van der Walt, R. Gommers, P. Virtanen, D. Cournapeau, E. Wieser, J. Taylor, S. Berg, N. J. Smith, R. Kern, M. Picus, S. Hoyer, M. H. van Kerkwijk, M. Brett, A. Haldane, J. F. del Río, M. Wiebe, P. Peterson, P. Gérard-Marchant, K. Sheppard, T. Reddy, W. Weckesser, H. Abbasi, C. Gohlke, and T. E. Oliphant, Array programming with NumPy, *Nature* **585**, 357 (2020).
- [57] P. Virtanen, R. Gommers, T. E. Oliphant, M. Haberland, T. Reddy, D. Cournapeau, E. Burovski, P. Peterson, W. Weckesser, J. Bright, S. J. van der Walt, M. Brett, J. Wilson, K. J. Millman, N. Mayorov, A. R. J. Nelson, E. Jones, R. Kern, E. Larson, C. J. Carey, I. Polat, Y. Feng, E. W. Moore, J. VanderPlas, D. Laxalde, J. Perktold, R. Cimrman, I. Henriksen, E. A. Quintero, C. R. Harris, A. M. Archibald, A. H. Ribeiro, F. Pedregosa, P. van Mulbregt, and SciPy 1.0 Contributors, SciPy 1.0: Fundamental Algorithms for Scientific Computing in Python, *Nature Methods* **17**, 261 (2020).
- [58] S. Lehtola, C. Steigemann, M. J. Oliveira, and M. A. Marques, Recent developments in libxc — a comprehensive library of functionals for density functional theory, *SoftwareX* **7**, 1 (2018).
- [59] mendeleev – a python resource for properties of chemical elements, ions and isotopes, ver. 0.9.0, <https://github.com/lmmentel/mendeleev> (2014–).
- [60] Joblib Development Team, Joblib: running python functions as pipeline jobs, <https://joblib.readthedocs.io/> (2020).
- [61] M. Pillai, J. Goglio, and T. G. Walker, Matrix numerov method for solving schrödinger's equation, *American Journal of Physics* **80**, 1017 (2012), <https://doi.org/10.1119/1.4748813>.
- [62] J. P. Perdew and Y. Wang, Accurate and simple analytic representation of the electron-gas correlation energy, *Phys. Rev. B* **45**, 13244 (1992).